BIOCHEMISTRY
including biophysical chemistry & molecular biology

Article

pubs.acs.org/biochemistry

Crystallographic Analysis of Active Site Contributions to Regiospecificity in the Diiron Enzyme Toluene 4-Monooxygenase

Lucas J. Bailey, Justin F. Acheson, Jason G. McCoy, Nathaniel L. Elsen, George N. Phillips, Jr., and Brian G. Fox*

Department of Biochemistry, University of Wisconsin, Madison, Wisconsin 53706-1544, United States

Supporting Information

ABSTRACT: Crystal structures of toluene 4-monooxygenase hydroxylase in complex with reaction products and effector protein reveal active site interactions leading to regiospecificity. Complexes with phenolic products yield an asymmetric μ-phenoxo-bridged diiron center and a shift of diiron ligand E231 into a hydrogen bonding position with conserved T201. In contrast, complexes with inhibitors *p*-NH_2-benzoate and *p*-Br-benzoate showed a μ-1,1 coordination of carboxylate oxygen between the iron atoms and only a partial shift in the position of E231. Among active site residues, F176 trapped the aromatic ring of products against a surface of the active site cavity formed by G103, E104 and A107, while F196 positioned the aromatic ring against this surface via a π-stacking interaction. The proximity of G103 and F176 to the *para* substituent of the substrate aromatic ring and the structure of G103L T4moHD suggest how changes in regiospecificity arise from mutations at G103. Although effector protein binding produced significant shifts in the positions of residues along the outer portion of the active site (T201, N202, and Q228) and in some iron ligands (E231 and E197), surprisingly minor shifts (<1 Å) were produced in F176, F196, and other interior residues of the active site. Likewise, products bound to the diiron center in either the presence or absence of effector protein did not significantly shift the position of the interior residues, suggesting that positioning of the cognate substrates will not be strongly influenced by effector protein binding. Thus, changes in product distributions in the absence of the effector protein are proposed to arise from differences in rates of chemical steps of the reaction relative to motion of substrates within the active site channel of the uncomplexed, less efficient enzyme, while structural changes in diiron ligand geometry associated with cycling between diferrous and diferric states are discussed for their potential contribution to product release.

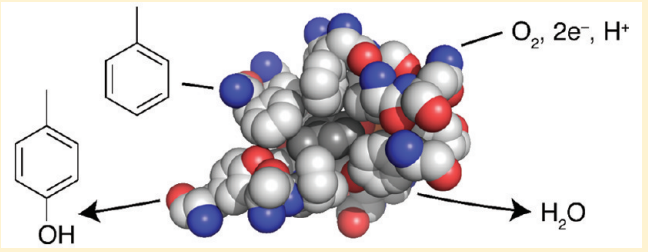

Diiron hydroxylases catalyze many different reactions, including the oxidation of unactivated C−H bonds,[1] stereospecific alkene epoxidation,[2] regiospecific aromatic ring hydroxylation,[3] phenolic oxidation,[4] and others. The steadily growing list of other diiron enzymes provides reactions with deoxyribonucleotides,[5] antibiotics,[6,7] fatty acids[8,9] and alkanes,[10] iron storage proteins,[11] and oxidases,[12,13] coenzyme Q biosynthesis[14] and post-translational modifications of tRNA,[15] cellular secondary messengers,[16] cell proliferation proteins,[17] and aging factors.[18] Arising from these myriad biological contributions, diiron enzymes are the subject of intense investigations that aim to create synthetic small molecules that mimic their catalytic properties[19−24] and, in the case of the aromatic ring monooxygenases, to employ them in bioremediation[25] or fine chemical synthesis.[26−30] Consequently, understanding the determinants of enzyme regio- and stereoselectivity can improve our understanding of the reaction mechanism[21,31] and also contribute to the design of engineered hydroxylases for specific purposes.

The aromatic ring diiron hydroxylases are multiprotein complexes.[32] In all, a flavin-containing oxidoreductase accepts reducing equivalents from NAD(P)H and transfers them to a [2Fe-2S] ferredoxin domain that is the proximal electron donor to the hydroxylase. In the three-protein complexes (e.g., methane monooxygenase), the oxidoreductase contains both flavin and [2Fe-2S] and so directly reduces the hydroxylase diiron center. In the four-protein complexes (e.g., T4MO and alkene epoxidase), a Rieske-type [2Fe-2S] ferredoxin serves as an intermediate electron carrier between the oxidoreductase and the hydroxylase. The diiron center and catalytic active site are entirely contained within the hydroxylase,[33−37] which has an $(\alpha\beta\gamma)_2$ quaternary structure. Hydroxylase function is dramatically enhanced by formation of a complex with a small cofactorless effector protein, which is manifested by increases in the rate of steady-state catalysis, coupling, O_2 activation, and other steps of the reaction cycle,[38] changes in the active site geometry,[37] and inhibition at high effector protein concentrations.[39−41]

T4MO oxidizes the natural substrate toluene with ∼97% regiospecificity for the *para* position.[42] Previous studies with T4MO and related diiron enzymes have shown that mutagenesis can alter the regiospecificity of the enzyme for reaction

Received: December 12, 2011
Revised: January 19, 2012
Published: January 20, 2012

   dx.doi.org/10.1021/bi2018333 | *Biochemistry* 2012, 51, 1101−1113

with toluene and other nonphysiological substrates,[30,43−47] in some cases with no deleterious changes in the catalytic properties of the purified enzymes[40,45,48] and in others with a broadened range of substrates reacted.[29,49−51] For example, G103L T4moH oxidizes toluene with ∼55% regiospecificity for the *ortho* position, a dramatic change from the natural enzyme, while also retaining equivalent kinetic parameters and coupling.[40]

The presence of the effector protein contributes to the high regiospecificity for hydroxylation found in some diiron hydroxylases,[2,40,52] expanding the molecular definition of catalytic outcomes to include the essential role of protein complex formation. High-resolution crystal structures demonstrating the extensive changes caused by stoichiometric binding of the effector protein[37,48] and in addition structures with some product analogues bound throughout the protein are now available.[35,53] However, none of these latter structures contained aromatic substrates or products in the active site.

Here we report crystal structures of T4moH alone bound to 4-Br-phenol (T4moH-BML) and the complexes of T4moH with effector protein T4moHD (T4moHD) bound to the natural product *p*-cresol (T4moHD-PCR), alternative products phenol (T4moHD-IPH) and *p*-nitrophenol (T4moHD-NPO), and inhibitors *p*-NH_2-benzoate (T4moHD-PAB) and bromobenzoate (T4moHD-BRB). This suite of structures show that the effector protein does not influence the residues contributing to the positioning of substrates and products and so has its predominant influence on the ligation geometry of the diiron center and its associated hydrogen bonding network.[37] In combination, these structures define the ways in which aromatic molecules are ultimately positioned in the active site and suggest how a simple mutagenic change in the cavity adjacent to the diiron center may contribute to a redistribution of products. Differences in the reactivity of diiron center intermediates relative to diffusional motions of substrates may thus yield the observed changes in product distributions as the effector protein is titrated into catalytic reaction mixtures.[40,52] Furthermore, structures presented herein provide insight into how movement of a diiron carboxylate ligand may facilitate product release upon reduction of a product-bound diferric center.

MATERIALS AND METHODS

Materials. Substrates, products, inhibitors, and other chemicals were from Aldrich (Milwaukee, WI).

Preparation of T4moH and G103L T4moH. Vector p58KABE was transformed into *Escherichia coli* BL21, and the cells were grown overnight at 37 °C on Luria-Bertani agar plates containing 50 μg/mL kanamycin.[54] A starting inoculum for the stirred vessel fermentation was prepared by placing a single colony into 2 mL of Luria-Bertani medium containing 50 μg/mL kanamycin. The 2 mL culture was incubated at 37 °C with shaking at 250 rpm until it reached an OD_{600} between 0.5 and 1 (this typically occurred after ∼8 h). Next, 1 L of Luria-Bertani medium with 50 μg/mL kanamycin was inoculated with 500 μL of the 2 mL culture and incubated overnight (∼12−14 h) at 25 °C while being shaken at 225 rpm. When the 1 L culture had reached an OD_{600} between 0.5 and 1, the 1 L culture was added to 9 L of sterilized Luria-Bertani medium with 50 μg/mL kanamycin in a Bioflo 3000 fermenter (New Brunswick Scientific, New Brunswick, NJ) and grown at 37 °C with agitation at 250 rpm. The dissolved content of O_2 was allowed to decrease to 20% of air saturation, and subsequently, the extent of agitation was allowed to increase under feedback control to maintain the dissolved O_2 content at 20% of air saturation. At an OD_{600} of ∼3, the temperature was decreased to 25 °C and 10 mL of 1 M IPTG (Fisher Scientific, Pittsburgh, PA) and 20 g of Casamino acids (Fisher Scientific) were added to the culture medium. After induction of protein expression, the growth of the culture continued for 4 h, and the OD_{600} reached ∼10. The cells were recovered by centrifugation at 4500*g* for 25 min at 4 °C in a JS-4.2 rotor and an AvantiTM J-HC centrifuge (Beckman Coulter, Fullerton, CA). The yield from this expression protocol was ∼8−10 g of wet cell paste per liter of culture medium. The cell paste was stored at −80 °C.

Cell pastes were resuspended in 25 mM MOPS (pH 6.9) containing 200 mM NaCl and 2% glycerol at a ratio of 1.5 mL/g of wet cell paste. The cell suspension was sonicated on ice at high intensity for 4 min (10 s on and 30 s off). The supernatant from the sonicated cells was recovered by centrifugation at 39200*g* for 60 min at 4 °C. The supernatant was carefully decanted and diluted with 2 volumes of the buffer described above and loaded onto a DEAE-Sepharose column (45 mm diameter × 250 mm, GE Healthcare, Piscataway, NJ) equilibrated in the buffer described above and eluted in a 200 to 450 mM NaCl gradient in the same buffer at a linear flow rate of 40 cm/h. Fractions were pooled on the basis of both activity and purity as determined by sodium dodecyl sulfate−polyacrylamide gel electrophoresis. Pooled fractions were concentrated and applied to a Sephacryl S-300 column (45 mm diameter × 1000 mm, GE Healthcare) equilibrated in the buffer described above at a linear flow rate of 5 cm/h. Fractions were pooled on the basis of activity and purity, concentrated to ∼1 mM active sites, and exchanged into 10 mM MOPS (pH 6.9) containing 200 mM NaCl. The purified protein was drop-frozen in liquid N_2 and stored at −80 °C.

Preparation of T4moC, T4moD, and T4moF. These protein components were expressed, purified, and characterized as previously described.[54−56]

Assays. Steady-state reactions with the reconstituted T4MO complex were performed as previously described.[40]

Crystallization. Crystals of resting T4moH were obtained from the small-scale batch method by addition of 5 μL of T4moH (∼95 μM) in 10 mM MOPS (pH 6.9) containing 200 mM NaCl to an equal volume of precipitant containing 0.1 M HEPES (pH 7.5), 15% MePEG 2000, 100 mM $CaCl_2$, and 20 mM NaN_3. Crystals grew to dimensions of ∼100 μm × 100 μm × 50 μm over ∼1 week at 22 °C. To obtain the T4moH-BML structure, T4moH crystals were soaked in mother liquor containing 10 mM 4-Br-phenol for approximately 15 min before cryoprotection. The T4moH-BML crystals were cryoprotected by immersion in Fomblin (molecular weight of 2500) and frozen in liquid N_2.

Crystals of T4moHD were obtained from hanging drop vapor diffusion by the addition of 2 μL of a solution of T4moH (140 μM) and T4moD (280 μM) in 10 mM MOPS (pH 6.9) containing 50 mM NaCl to an equal volume of precipitant containing 100 mM Bis-Tris (pH 6.0), 20−24% (w/v) PEG 3350, and 200 mM NH_4Cl. To obtain the T4moHD−PAB crystals, 100−200 mM *p*-NH_2-benzoate was included in the precipitant. To obtain the T4moHD−IPH crystals, a 2× precipitant buffer containing 100 mM phenol was prepared, and 250 μL of this solution was added to each crystallization well along with 250 μL of PEG 3350 prepared in deionized H_2O. To obtain the T4moHD−NPO crystals, a precipitant solution containing 16 mM *p*-nitrophenol was prepared; 250 μL of this solution was added to each crystallization well along with 250 μL of PEG 3350

prepared in deionized H_2O to a final concentration of 20−24%. Similarly, to obtain T4moHD−PCR crystals, a precipitant solution containing *p*-cresol (160 mM) was prepared; the nominal concentration of *p*-cresol in the mother liquor was 40 mM. Crystals were cryoprotected with Fomblin 2500 and were frozen in liquid N_2.

Crystals of G103L T4moHD were obtained from hanging drop vapor diffusion by the addition of 2.5 μL of a solution of T4moH (140 μM) and T4moD (280 μM) in 10 mM MOPS (pH 6.9) containing 50 mM NaCl to an equal volume of precipitant containing 100 mM Bis-Tris (pH 6.5), 21% (w/v) PEG 3350, and 200 mM sodium acetate. Crystals grew to ∼200 μm × 200 μm × 200 μm after ∼1 week at 22 °C. Crystals were cryoprotected by incubation in 3% increments of PEG 3350 to a final concentration of 27% and were frozen in liquid N_2.

Structure Determination. Diffraction data were collected at GMCA-CAT, beamline 23-ID, and LS-CAT, beamlines 21-ID-F and -G, at the Advanced Photon Source, Argonne National Laboratory (Argonne, IL). Diffraction data for T4moHD−PAB, T4moHD−Z82, T4moHD−NPO, and T4moHD−IPH crystals were collected at LS-CAT beamline 21-ID-G. Diffraction data for T4moHD−PCR crystals were collected at LS-CAT beamline 21-ID-F. Diffraction data were indexed, integrated, and scaled using HKL2000.[57] The structure of the resting T4moH−BML complex was determined by molecular replacement with the CCP4 suite program MOLREP[58] using resting T4moH structure 3DHG as the starting model. The structures of G103L T4moHD and the T4moHD product−inhibitor complexes in space group *C*2221 were determined by molecular replacement[58] using resting T4moHD structure 3DHH, while the T4moHD−Z82 structure in space group $P2_12_12_1$ was determined using resting T4moH structure 3DGH. Electron density was fit and refined using Coot,[59] REFMAC5,[60] and/or PHENIX.[61] TLS refinement was also employed in refinement with PHENIX. Ramachandran analysis and rotamer analysis were performed with Molprobity.[62] Analysis of active site tunnels was done using Caver.[63] Figures were prepared using PyMOL.[64]

RESULTS

Structure Determination. Statistics from the structure determinations are listed in Table 1. The T4moH−BML, T4moHD−PCR, T4moHD−IPH, T4moHD−NPO, T4moHD−Z82, T4moHD−PAB, and T4moHD−BML crystal structures were determined to resolutions of 1.95, 1.75, 1.95, 1.84, 1.75, 1.99, and 1.94, respectively. BML, PCR, IPH, and NPO are products of the reaction of T4moHD with bromobenzene, toluene (k_{cat} = 2.0 s^{-1}), benzene (k_{cat} = 0.8 s^{-1}), and nitrobenzene (k_{cat} = 0.13 s^{-1}), respectively, while PAB is an inhibitor of toluene oxidation ($K_i \approx 5$ μM). These are the first structures showing aromatic molecules bound to the diiron center in a hydroxylase active site. The structure of G103L T4moHD was also determined at a resolution of 2.10 Å.

Structural Alignments. The protomer of diiron hydroxylases consists of three polypeptide chains that are further assembled into a dimeric quaternary structure. The protomer of T4moH consists of the TmoA (55 kDa, containing the diiron center), TmoB (10 kDa), and TmoE (35 kDa) polypeptide chains; in the following, we consider alignments of the protomer structures. When aligned using all atoms, the T4moH and T4moH−BML protomers had an ∼0.2 Å rmsd. Moreover, the T4moH protomer aligned with the protomers of either T4moHD or T4moHD−PCR with an ∼0.3 Å rmsd, with the slightly increased mismatch ascribed to rearrangements of a small portion of the TmoA polypeptide caused by T4moD binding.[37] Furthermore, all structures of the T4moHD complex reported here, including G103L T4moHD and the various structures with bound aromatic molecules, aligned with a <0.15 Å rmsd over the entire protomer. Thus, neither exposure to aromatic molecules at concentrations of up to 0.2 M nor the active site mutation produced significant changes in the folding in either T4moH or T4moHD other than those already assigned to complex formation.

Aromatic Molecule Binding Sites. Figure 1 shows a composite of positions where aromatic molecules have been identified in resting T4moH and T4moHD (this work) and in the closely related toluene/*o*-xylene monooxygenase, ToMOH.[35] There is considerable overlap in these binding sites among the individual structures. An extended cavity (site 1) created by the loop between helix αI of TmoA and the loop connecting β1 and β2 of TmoB contained BML, PCR, IPH, NPO, PAB, or Z82 in the various structures. Aromatic molecules were also bound in a smaller cavity in the interface between the TmoA and TmoE chains (site 2, containing BML or IPH). There are no reasonable direct connections from where these aromatic molecules reside into the active site.

Aromatic molecules (BML and PCR) were also observed in the interface between T4moH and T4moD (Figure 1, site 3, and Figure 2, PDB entry 3Q14). The interstitially bound PCR-6029 was within 4 Å of R6, Y51, and K52 of TmoA and also within 4 Å of M74, Q75, L77, A90, and I95 of T4moD. I88 of T4moD makes contacts with Y51 of TmoA and thus repositions it in the protein−protein complex.[37] Similar contacts were observed for BML-1912 in the T4moHD−BML structure (not shown, PDB entry 3DHH).

Active Site Access. In both ToMOH (PDB entry 1T0S[35]) and T4moH (PDB entry 3DGH[37]), a prominent tunnel passes from the surface through ∼30 Å of the protein interior to reach the active site. Aromatic molecules were observed along this tunnel and in a chamber adjacent to the active site in both enzymes (Figure 1, site 4) (site 4 defined here for T4moH overlaps with sites 2 and 3 assigned earlier in TomoH[35]). In T4moH, these product molecules (BML-496 in chain A and BML-497 in chain D of PDB entry 3RMK) were ∼12 Å from the diiron center and appear to occupy a proximal site for substrate−product binding along the main tunnel. The entrance to the active site of T4moH-BML is shown in Figure 3. Table S1 of the Supporting Information lists the T4moH active site residues and iron ligands that were within ∼4 Å of the aromatic molecules bound to the diiron center, which corroborates earlier assignments of the active site based on homology modeling.[43,44] There is a remarkable conservation of these residues among the different diiron hydroxylases, with substitutions of residue types or shifts in positions observed in only a few instances, yet distinct distributions of products arise from reactions of the same substrates.

Active Sites Bound with Phenolic Products. The coordination geometry in the active site of T4moH-BML is shown in Figure 4. This structure represents a product complex that would be obtained from reaction of bromobenzene. The residues identified in Table S1 of the Supporting Information and others create the inner surface of the T4moH active site cavity. In the T4moH−BML structure, the BML molecules were modeled at 70% occupancy in both active sites of the dimer, and the average *B* factors of the BML atoms were ∼20 $Å^2$. Although these *B* factors were slightly higher than those observed for the other iron ligands, the side chains of several

dx.doi.org/10.1021/bi2018333 | *Biochemistry* 2012, 51, 1101−1113

Table 1. Summary of Data Collection, Crystal Structure, and Refinement Statistics[a]

	T4moH−BML	T4moHD−PCR	T4moHD−IPH	T4moHD−NPO	T4moHD−Z82	T4moHD−PAB	T4moHD−BML	G103L T4moHD
aromatic ligand	4-Br-phenol	*p*-cresol	phenol	*p*-nitrophenol	4-Br-benzoate	p-NH_2-benzoate	4-Br-phenol	none
PDB entry	3RMK	3Q14	3Q3O	3Q3N	3Q3M	3Q2A	3DHH	3RI7
space group	$P2_12_12_1$	$C2221$	$C2221$	$C2221$	$P2_12_12_1$	$C2221$	$C2221$	$C2221$
resolution (Å)	43.0−1.95 (2.00−1.95)	38.70−1.75 (1.81−1.75)	31.7−1.95 (2.02−1.95)	29.1−1.84 (1.91−1.84)	34.09−1.75 (1.78−1.75)	29.2−1.99 (2.06−1.99)	91.29−1.94 (2.01−1.94)	39.19−2.10 (2.16−2.10)
completeness (%)	99.3 (95.67)	89.4 (75.6)	92.5 (71.0)	93.6 (75.0)	93.6 (87.6)	92.4 (72.0)	99.4 (97.5)	99.57 (95.58)
no. of reflections	123099	104364	70524	83883	198404	65774	77871	62329
R value (working)[b]	0.157 (0.223)	0.148 (0.226)	0.150 (0.189)	0.151 (0.222)	0.143 (0.207)	0.141 (0.175)	0.157 (0.180)	0.168 (0.274)
R_{free}[c]	0.196 (0.282)	0.175 (0.226)	0.192 (0.254)	0.188 (0.285)	0.178 (0.246)	0.188 (0.274)	0.202 (0.257)	0.213 (0.319)
mean *B* value (Å^2)	15.8	25.31	34.9	31.1	17.4	36.4	25.5	32.6
R_{merge}	0.118 (0.527)	0.071 (0.481)	0.050 (0.318)	0.073 (0.449)	0.101 (0.556)	0.070 (0.393)	0.054 (0.203)	0.077 (0.630)
no. of non-hydrogen atoms[d]	14432	9094	8784	8984	18516	8943	8972	8866
no. of solvent molecules	1565	849	611	714	2125	704	766	662
Ramachandran plot (%)								
favored	98.1	96.6	96.6	96.2	96.5	96.1	92.2	97.9
additionally allowed	1.8	3.3	3.4	3.7	3.3	3.8	7.6	2.1
disallowed	0.1	0.1	0	0.1	0.2	0.1	0.1	0.0
rmsd								
bond lengths (Å)	0.008	0.006	0.006	0.006	0.011	0.007	0.015	0.006
bond angles (deg)	1.020	1.041	0.993	1.012	1.231	1.000	1.392	0.934

[a]Numbers in parentheses are data for the highest-resolution shell. [b]$R = \sum||F_o| - |F_c||/\sum|F_o|$, where F_o is the observed structure factor amplitude and F_c is the calculated structure factor amplitude. [c]R_{free} is the *R* factor calculated on the basis of exclusion of ~5% of the data from the refinement. [d]Number of non-hydrogen atoms included in refinement, including water molecules.

dx.doi.org/10.1021/bi2018333 | *Biochemistry* 2012, 51, 1101−1113

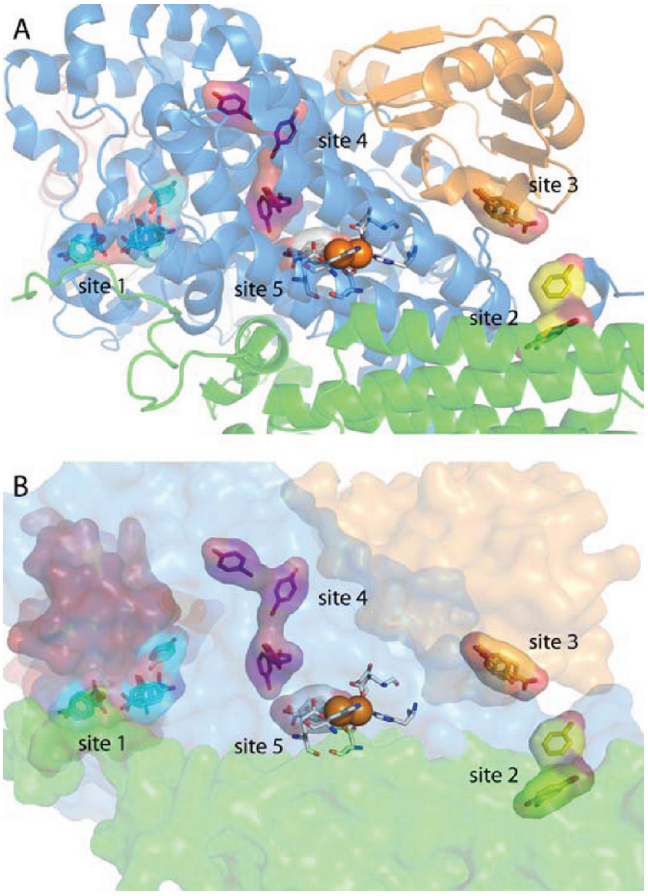

Figure 1. Locations of aromatic products bound to T4moH and T4moHD. (A) Cartoon representations of the TmoA, TmoB, and TmoE subunits and T4moD colored blue, red, green, and orange, respectively. (B) Transparent surface representations with the same color coding as in panel A. Site 1 lies between the TmoA and TmoB subunits. Site 2 is contained in the TmoE subunit. Site 3 is between the TmoA and TmoD subunits; PCR, BML, and Z82 were identified in this site. Site 4 corresponds to the active site tunnel;[37] three BML molecules shown as sticks were identified in the tunnel in toluene/*o*-xylene monooxygenase (PDB entry 1T0S[35]), and additional orientations of BML were identified in T4moH. Site 5 is the inner cavity of the active site. PCR, BML, IPB, PAB, and Z82 have been identified in this site.

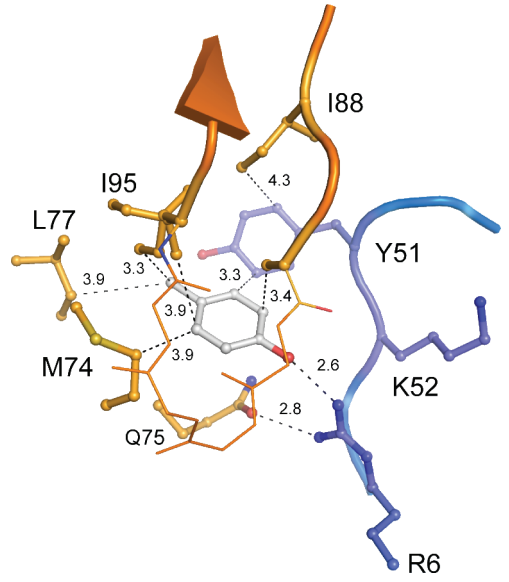

Figure 2. Binding of PCR (white sticks) at site 3 in the interface between the TmoA subunit of T4moH (blue) and T4moD (orange). Interatomic distances described in text are indicated.

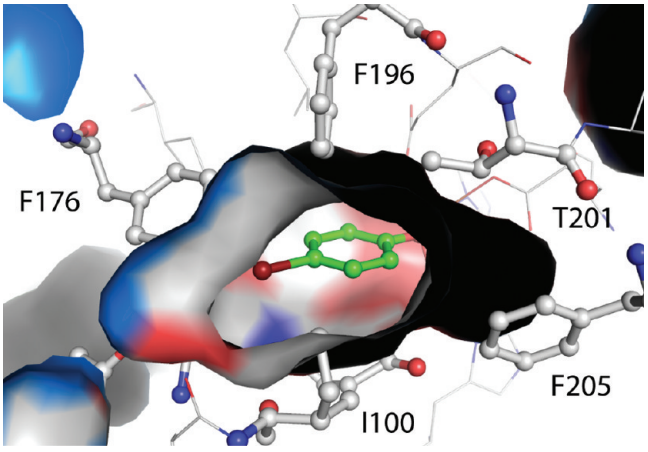

Figure 3. Residues creating the surface of the cavity surrounding BML (green sticks) bound to the diiron center in T4moH-BML (PDB entry 3RMK). Residues G103 and E104 provide a flat surface that contacts the aromatic ring, while residues F176 and F196 interact with the *para* substituent and the π-system of the aromatic ring, respectively. Residues I100, T201, and F205 are near the cavity but are not in contact with the bound product.

hydrophobic residues that create the active site surface in the vicinity of the diiron center had comparable *B* factors. The ~70% occupancy observed for BML in the active site of the T4moH–BML structure may have resulted from the short soaking time that was required to prevent significant degradation of the fragile resting T4moH crystals.

Ligand-to-metal charge transfer observed at ~600 nm from T4moH treated with BML in solution and the purplish hue of the crystals suggested that this product was bound as phenolate; a similar conclusion was reached in spectroscopic studies of methane monooxygenase mixed with phenol.[65] The phenolate O atom occupies a μ-1,1 bridging position between the iron atoms and thus displaces either the water or hydroxo bridge (HOH1) found in resting T4moH at this position. The bridging phenolate O atom is bound asymmetrically, with an Fe1–O distance of 2.7 Å and an Fe2–O distance of 2.0 Å. The iron atoms in the resting T4moH and T4moH–BML structures are separated by ~3.2 Å, so the presence of the phenolate bridge did not alter the Fe–Fe distance. The aromatic ring of BML makes contacts with portions of the side chains from G103, E104, A107, E134, F176, I180, and F196. For comparison, the methoxy (PDB entry 1FZ6), ethoxy (PDB entry 1FZ7), and Br-ethoxy (PDB entry 1XVG) groups bridging the ferric sites in the respective methane monooxygenase structures have more symmetric bonding with distances in the range of 1.9–2.1 Å;[53,66] these small bridging ligands do not make contacts with distal residues in the active site.

Preformed T4moHD crystals soaked with BML yielded structures with this molecule present in several of the exterior cavities shown in Figure 1, but no BML molecules were observed in either site 4 or site 5 within the protein (PDB entry 3DHH). This suggested access to the active site was restricted in the closed conformation of preformed T4moHD crystals.

dx.doi.org/10.1021/bi2018333 | *Biochemistry* 2012, 51, 1101–1113

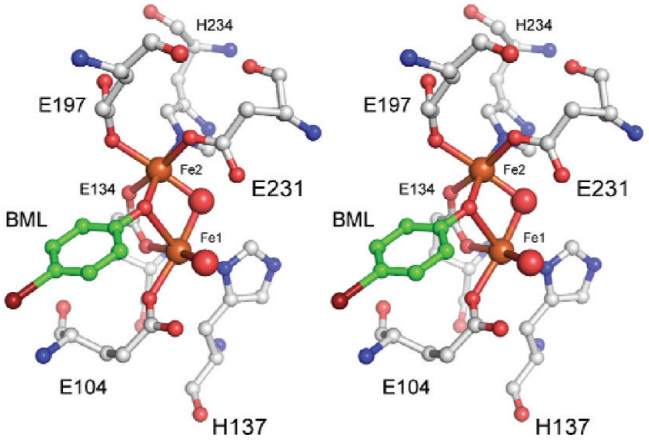

Figure 4. Cross-eyed stereo image of the active site of T4moH bound with BML (PDB entry 3RMK).

Alternatively, crystallization of T4moH and T4moD with either PCR (Figure 5, 1.68 Å) or other products added to the crystallization solutions yielded structures with an aromatic molecule bound to the diiron center. When compared to the T4moH−BML structure, the various product-bound T4moHD structures showed nearly identical placement of the phenolate O atom, including the asymmetry of bond lengths between the bridging phenolate and the iron atoms (Figure 6A). Moreover, active site water HOH5 localized by effector protein binding[37] was found in a nearly identical position in each of the phenolate product structures when an effector protein was present, but HOH5 was not found in the T4moH−BML structure.

Active Sites Bound with Inhibitors. T4moHD cocrystallized in buffer containing the reaction inhibitors 4-Br-benzoate [Z82, PDB entry 3Q3M (Figure 7)] and *p*-NH_2-benzoate (PAB, PDB entry 3Q2A) also yielded structures with the aromatic compound within the active site and bound to the diiron center. The positions of the iron-bound inhibitors were nearly identical, as one carboxylate O atom bridged the iron atoms (Figure 6B, ~2.3 Å to Fe2 and ~2.6 Å to Fe1) in a position nearly identical to that of the phenolate O atom. Notably, unlike the resting T4moHD and the phenolate-bound structures described above, E231 did not rotate into a hydrogen bonding position with T201 when the inhibitors were present. Instead, E231 was asymmetrically

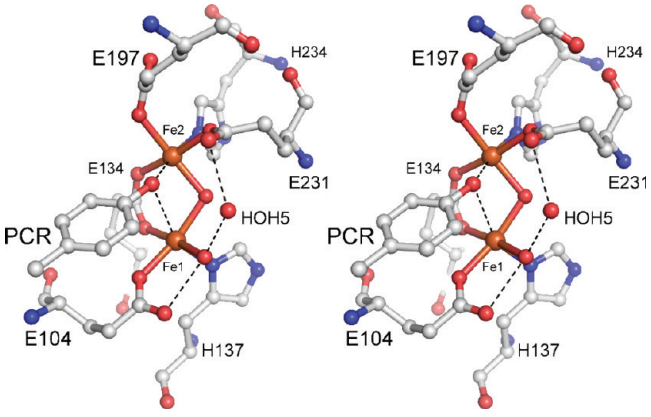

Figure 5. Cross-eyed stereo image of the diiron coordination sphere in T4moHD bound to *p*-cresol (PCR, PDB entry 3Q14). PCR is bound as an asymmetric μ-1,1 phenoxide bridge. HOH5 was observed in all phenolate-bound structures in which T4moHD was also present.

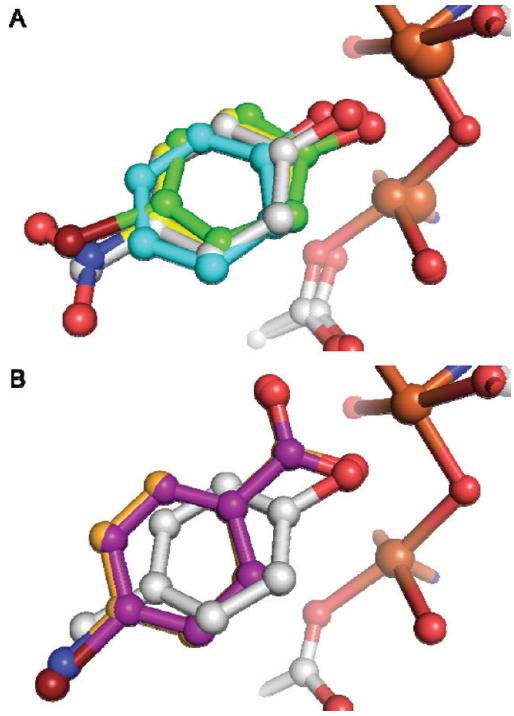

Figure 6. Overlay of structures showing (A) phenolic and (B) inhibitor complexes of T4moHD: PCR, white; IPH, cyan; NPO, yellow; Z82, purple; PAB, orange (PDB entries 3Q14, 3Q3O, 3Q3N, 3Q3M, and 3Q2A).

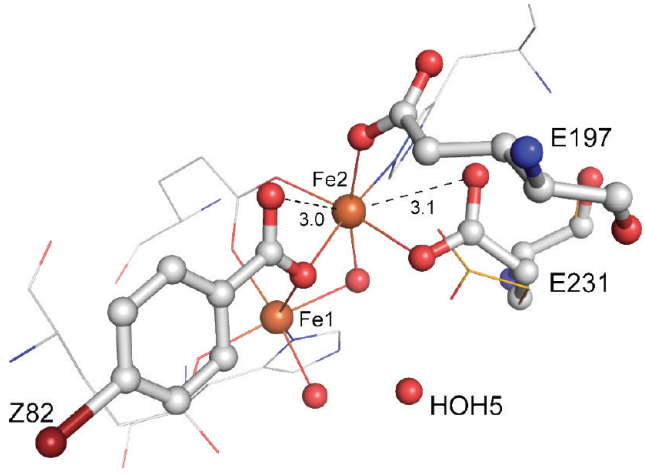

Figure 7. Structure of the active site of T4moHD bound with inhibitor Z82 (PDB entry 3Q2A). Z82 is bound in a μ-1,1 bridging mode by one carboxylate O atom, while the other O atom is 3.0 Å from Fe2. With Z82 bound, iron ligand E231 did not shift into the hydrogen bonding position with T201 that is characteristic of the T4moHD complex (the fully shifted position of E231 in T4moHD in the absence of inhibitor is shown as orange lines). HOH5 is present in the active site, as in all other structures of the T4moHD complex.

coordinated to Fe2 (~2.3 and ~3.1 Å to Fe2), mirroring the coordination mode of the inhibitor on the opposite side of the metal (~2.0 and ~3.0 Å to Fe2). The positions of the other diiron center ligands E104, E134, H137, E197, and H234 were unchanged in the inhibitor complexes relative to the resting T4moHD complex (PDB entry 3DHH). Likewise, the Fe−Fe distance was maintained at 3.2 Å, and HOH5 was observed in a nearly identical location. Because of the different coordination with respect to Fe2

dx.doi.org/10.1021/bi2018333 | *Biochemistry* 2012, 51, 1101−1113

and possibly the increased size of the inhibitor, the positions of the aromatic rings in Z82 and PAB were rotated relative to the position of the phenolic aromatic rings (Figure 6B, which show bound PCR for comparison) and were within 4.2 Å of several residues beyond those identified for the smaller phenolic molecules (Table S1 of the Supporting Information). Most of these additional residues were located at the opposite end of the active site cavity, away from the diiron center.

Assignment of Roles of Active Site Residues. Alignment of the structures presented here defines key interactions of active site residues with products (Figure 8A) and, by inference, the substrates. Thus, F176 (green sticks) interacts with the *para* substituent of the aromatic ring to hold the substrate against the surface provided by G103, E104, and A107 (blue sticks and dots). Also, F196 (green sticks) provides a π-stacking interaction with the aromatic ring of the bound product, which serves to accurately position the substrate relative to the diiron center. The interplay between F196 and a bound substrate may also influence the position of E197 (white sticks), corresponding to the predicted role of this residue in O_2 activation.[67] Furthermore, F205 (green sticks) provides a π-bonding interaction with HOH5 (red sphere and dots) opposite to the hydrogen bond network provided by T201 (yellow sticks), Q228 (purple sticks), and E231, which together position HOH5 adjacent to the diiron center. I100 (white sticks) is at the outer edge of the active site, but in a position where mutated residues may still be oxidized via long-range electron transfer[68] or where larger residues may interact with more closely bound substrates and thus change the specificity of hydroxylation.[51]

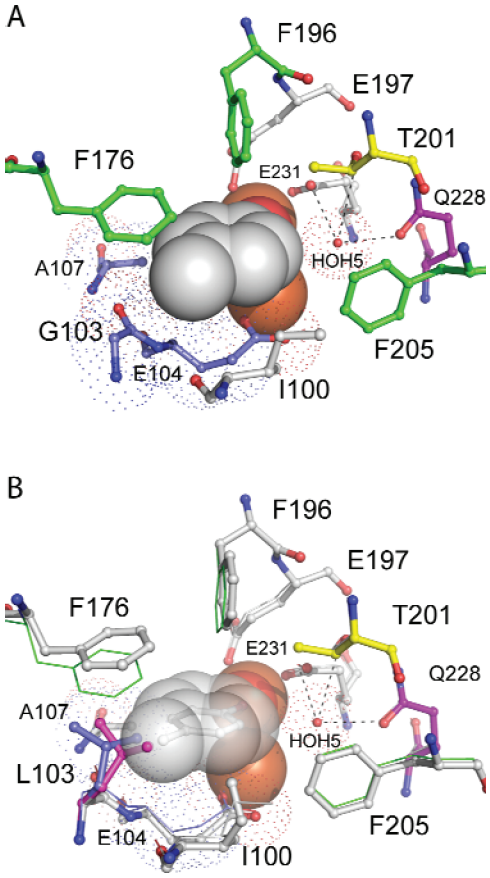

Figure 8. T4moH residues that form the active site, including binding pockets for substrate and/or products and HOH5. The roles of individual residues are described in Assignment of Roles of Active Site Residues. (A) T4moHD–PCR structure (PDB entry 3Q14) showing *p*-cresol bound in the active site. (B) G103L T4moHD structure (PDB entry 3RI7) showing a predicted overlap of one rotamer conformation of the introduced leucine residue (magenta sticks) with the *para* substituent of *p*-cresol in the aligned active site from panel A. The positions of I100 and F176 are shifted slightly between the G103L T4moHD (stick representation) and T4moHD–PCR (green lines) structures.

Active Site of G103L T4moHD. The structure of the active site cavity in G103L T4moHD is shown in Figure 8B. The positions of the iron atoms and coordinating ligands in G103L T4moHD superimposed with resting T4moHD. Moreover, helix αB, containing L103 and E104, did not change configuration upon mutation.[37] Indeed, the only significant changes were the presence of L103 in the active site cavity and slight shifts in the position of I100 and F176 to accommodate the newly introduced side chain (green sticks show positions in resting T4moHD). The L103 side chain adopted two rotamer conformations (blue and magenta) that are commonly observed in protein crystal structures.[69] These conformations had equal 50% occupancy and *B* factors (~20 Å^2) that were comparable to those of other active site residues. As observed in most other diiron hydroxylase structures (e.g., PDB entries 1MMO, 3DGH, etc.), acetate from the crystallization buffers bridged the iron atoms (not shown in the figure).

Upon alignment of the G103L T4moHD and T4moHD–PCR structures and those of other product complexes (Figure 8B), it became apparent that the L103 side chain would generate a steric clash with the *para* substituent of bound aromatic rings (H_3C in PCR, Br in BML and Z82, O_2N in NPO, and H_2N in PAB). More specifically, in rotamer conformation A of L103 (blue sticks), CD2 overlapped with the position of these substituents and may thus displace the *para* substituent toward the open space in the active site closer to I180, F196, and E197. This repositioning of the aromatic ring substituent may correspond to the ~55% *ortho* hydroxylation observed from G103L T4moHD. In contrast, conformation B of L103 (magenta sticks) has CD1 and CG oriented away from the position of the *para* substituent, suggesting a weaker influence on substrate repositioning and perhaps permitting the observed 35% retention of *para* hydroxylation.

DISCUSSION

Access to the Active Site. The structures of five diiron hydroxylases have been determined.[33−37] In all, the diiron center is buried ~12−14 Å below the nearest protein surface, raising the question of how substrates and products, which will include both the aromatic compound and O_2, enter and leave the active site. These structures reveal a number of internal cavities and/or tunnels, suggesting several possible routes, although their positions differ somewhat among the enzymes.[37,53,66,70] For aromatic substrates, methane monooxygenase crystals soaked with BML, 4-F-phenol, or IPH had a single aromatic ligand bound away from the active site in an internal cavity of the MmoA subunit.[53] This cavity does not exist in T4moH but instead roughly aligns with the buried residue Y260 of TmoA.

Structures of resting ToMOH[35] and later resting T4moH[37] revealed a contiguous ~30 Å tunnel extending from the surface into the active site, along with both inner and intermediate

dx.doi.org/10.1021/bi2018333 | *Biochemistry* 2012, 51, 1101−1113

chambers along the tunnel (Figure 1). Mutagenesis studies with ToMOH supported the viability of its main tunnel as a catalytically relevant path[50] for hydrocarbons, as does the crystallographic evidence showing occupation by relevant aromatic molecules. The open access of the main tunnel in T4moH crystals allowed BML to enter the active site of these crystals, while in contrast, structures of uncomplexed ToMOH and MmoH did not show aromatic molecules in the active site.[35,53] T4moD binding closed the main access tunnel in T4moH,[37] and consequently, efforts to soak preformed T4moHD crystals with different aromatic compounds failed to yield structures with these products in the active site even if these compounds were readily entrained elsewhere in the protein. Apparently, complex formation may serve to isolate the active site and trap any enclosed substrates for subsequent catalysis.

For gaseous substrates like CH_4 and O_2, a series of disconnected internal hydrophobic cavities in MmoH that were occupied by Xe and other substrate analogues originally suggested a path for diffusion into the active site.[66] More recently, the role of internal cavities in the migration of O_2 into the diiron active site has been elucidated by systematic variation of the dimensions of the cavities in ToMOH[70] and later phenol hydroxylase.[71] Thus, mutation of residues I100 and L272 in ToMOH, which are conserved in T4mOH, produced a dramatic decrease in the rate of formation of the diagnostic peroxo chromophore in T201S ToMOH.

There are other internal cavities within T4moH that might be involved in access and egress. One lies along αE and αF, facing toward the surface residues N202 and Q228. A traverse of this 11 Å cavity would provide the shortest possible path between the active site and the surface; however, hydrogen bonds between the side chains of N202 and Q228 block access, and no aromatic products have been identified in this cavity by crystallography. Furthermore, although T4moD binding caused substantial rearrangements of N202 and Q228, no route of entry into the active site was observed. Alternatively, in the structure of the complex of phenol hydroxylase and effector protein PHM (2INN, 2.7 Å; 2INP 2.3 Å[36]), a short tunnel linking the diiron center to the surface was observed in the interface. It is interesting to note that residues N204 and Q230 of phenol hydroxylase line the small tunnel that emerges into the interface of the phenol hydroxylase complex. These residues are comparable in sequence positions to N202 and Q228 of T4moH, but their positions do not align well in the structures. Because the hydrogen bonding interactions of residues comparable to N202 and Q228 from T4moH are not consistently observed in the other uncomplexed diiron hydroxylase structures, it is possible that structural variations at this position may provide opportunities for specialization of substrate entrance (e.g., toluene versus phenol) or product exit (p-cresol versus catechol).

Substrate Activation of Catalysis. Results with diiron hydroxylases indicate that the presence of substrates contributes to the reactivity of diiron intermediates. For example, the rate of decay of diferryl species compound Q produced by methane monooxygenase increased as the concentration of methane was increased,[72] while the presence of alkenes and aromatic compounds stimulated the decomposition of peroxodiferric compound P.[73,74] T201A T4moH stoichiometrically released H_2O_2 in the absence of substrate but nevertheless became a fully coupled monooxygenase in the presence of substrate, implicating the importance of proximity between the substrate and reactive intermediates.[48] Furthermore, *p*-xylene predominantly yielded benzylic oxidation instead of aromatic hydroxylation,[43,75] suggesting that steric interactions might influence the substrate or reactive intermediates, leading to the shift to benzylic hydroxylation. Because the substrate is positioned by interaction with F196, changes in this interaction will presumably be transmitted to adjacent iron ligand E197, where subtle changes in configuration geometry have been previously implicated in O_2 activation.[67]

While there is no apparent pathway for movement of aromatic molecules from the interface between T4moH and T4moD into the active site of T4moHD (Figure 3), the presence of BML, PCR, and other aromatic molecules in this interstitial space is intriguing. Product PCR-6029 seen in the interface between T4moH and T4moD was not near T4moH residues N202 and Q228, which undergo substantial rearrangements upon complex formation. Instead, PCR-6029 is near T4moH residue Y51, which undergoes the largest distance excursion of any T4moH residue upon complex formation. One possibility is that occupation of this binding site may provide a physical mechanism for improved coupling between the presence of substrates and the conformational changes needed for activation of the enzyme catalysis. Along this line of reasoning, when methane monooxygenase effector protein (MmoB) residues that align with I88 of T4moD were mutated to smaller residues, an increased rate of product formation was obtained in single-turnover studies with larger substrates.[76] It is possible that larger substrates occupied the cavity created by the MmoB mutagenesis and thus influenced the methane monooxygenase interface. We also note that F60 of MmoA is related in sequence position to Y51 of TmoA, and that F60 lies adjacent to a tunnel traversing the MmoA subunit, offering an open space to accommodate MmoB-induced rearrangements.

Residues Contributing to Regiospecificity. Mutagenesis has been successfully used to alter the catalytic specificity of many diiron hydroxylases. Pikus and co-workers first showed the ability to change regiospecificity by mutagenesis of predicted T4moH active site residues.[43] Mitchell and co-workers later showed that changes at G103 could strongly alter regiospecificity without a loss of catalytic performance[40] and also noted that the natural diversity of residues at that position in the diiron hydroxylase active site could arise from changes in the third position of the corresponding codon. In G103L T4moHD, the near identity in positions of diiron center ligands and HOH5 likely accounts for the high level of catalytic performance. However, the two rotamer conformations observed for L103 in G103L T4moH (Figure 8B) also plausibly interact with aromatic ring substituents in different ways and thus might play a role in dictating regiospecificity through the half-occupancy assigned to the L103 rotamer in conformation A (blue sticks in Figure 8B). Other naturally occurring *ortho* hydroxylating diiron hydroxylases have moderately sized residues at the active site position comparable to those of G103L T4moH, with both T2moH[77] and phenol hydroxylase (Table S1 of the Supporting Information) also having a leucine residue at this position, and with both of these enzymes preferentially yielding *ortho* hydroxylation. Interestingly, ToMOH,[78] which has a relaxed hydroxylation regiospecificity, has a glutamate residue at the comparable position.[35] In the resting structure of ToMOH (PDB entry 1T0S), the carboxylate side chain projects away from the active site and forms a hydrogen bond in the interface between the A and B chains with B chain residue Y31. This residue will presumably remain fixed in position according to the results presented here, as no major active site rearrangements were observed under the influence of products and effector protein.

The origins of how G103 and A107 influence regiospecificity are better defined by this work. These structures show that these

residues provide a surface upon which the aromatic molecule is positioned by F176 and F196 (Figure 8), potentially defining a four-site combinatorial problem. Previously, Tao and co-workers reported the production of 1-hydroxyfluorene using G103S/A107G T4moH obtained by a directed evolution process.[51] This variant also gave greater than 80% *ortho* hydroxylation of toluene, similar to the result reported for G103L/A107G T4moH.[79] In the T4moHD−PCR structure, the methyl side chain of A107 was ∼3.6 Å from C3 of PCR (Figure 5) and maintained this approximate distance in the complexes of T4moHD with the other phenolic products. The A107G mutation likely altered the presentation of C3 for oxidation, perhaps by allowing rotation of the substrate methyl substituent toward the position normally occupied by the side chain methyl group.

Structures presented herein indicate that F196 provides a critical π-stacking interaction with the bound aromatic molecules. When T4moD bound, the F196 phenyl group moved by ∼1 Å,[37] representing the largest motion by a nonligand residue in the active site. Because F196 is adjacent to Fe2 ligand E197, changes in the conformation of F196 may subtly influence the configuration of E197 through steric interactions. Changes in the configuration of E197 have been implicated in O_2 activation[67] and may thus be successively linked to the presence of substrates by their interactions with F196. As further support for the involvement of F196, this residue moved ∼2 Å closer to the diiron center in T201A T4moHD, which has an increased rate of single-turnover catalysis.[48] This shift presumably changed π-stacking interactions, which could potentially move the substrate closer to the diiron center or alter its trajectory toward reactive intermediates, providing some possible mechanisms for increasing the rate of single-turnover catalysis.

Structure of Inhibitor Complexes. In the presence of inhibitors Z82 and PAB, diiron center ligand E231 did not shift into the hydrogen bonding position with T201 observed in other T4moHD structures (Figure 7). Instead, the carboxylate groups from E231 and the inhibitor assumed similar coordination geometries across opposite sites of Fe2. Otherwise, there was no change in the Fe−Fe distance or the position of other iron ligands and distal active site residues in these inhibitor complexes relative to those of other T4moHD structures. Among other diiron enzyme structures, E243 of methane monooxygenase had a configuration similar to that of E231 of T4moHD in crystals poised in a mixed-valence state (PDB entry 1FZ0[66]) and in crystals grown in the presence of DMSO (PDB entry 1FZ2), but in each of these structures, the Fe−Fe distance was increased relative to that in the diferric resting state.

Active Site-Bound Phenolic Products. Given the high degree of complementarity of the T4moH active site for the various aromatic compounds studied here, it is likely that toluene and other monosubstituted aromatic ring substrates will bind in a similar fashion. With aromatic substrates, close approach of the aromatic ring to the diiron center during the O atom transfer step of the catalytic reaction likely contributes to the high fidelity of isotopic incorporation.[45]

The asymmetric binding of PCR and other phenols is comparable to the asymmetric binding of azide observed in both ToMOH (PDB entry 1T0R[35]) and T4moH (PDB entry 3DHG[37]). In the 3DGH structure, azide N1 was bound in a μ-1,1 bridging position and was 2.3 Å from Fe2 and 2.6 Å from Fe1. Upon alignment of resting T4moH containing the bridging azide with the PCR-bound structure reported here, the N1 atom of azide and the O atom of *p*-cresol overlap, suggesting that accommodation of a μ-1,1 peroxodiferric configuration would require a positioning of the substrate that is hard to visualize given the tight spatial constraints of the active site revealed by these structures. The product-bound structures also suggest a specific location where a μ-1,2 peroxodiferric species[74,80] and/or diiron-bound oxene[81] might reside prior to reaction with substrate. Interestingly, the positioning of the μ-1,2 peroxide shown in T4moHD[80] would not generate unfavorable steric interactions with substrates if the product-bound structures are used as a guide.

Because of the limited changes in positions of active site residues other than E231, and also the tight constraints around the aromatic product in the presence or absence of effector protein, we now consider that the previously reported changes in product distributions in the absence of effector protein[2,40,52] are most likely to arise from differences in rates of chemical steps of reaction relative to motions of substrates within the active site tunnel of the uncomplexed, less efficient enzyme. This may include alternative configurations caused by diffusional motions of the substrate, conversion between unbound and effector protein-bound states of the hydroxylase, and reactions of different oxidation states of the active site ensemble.

Product Release. The exact order of the many interactions required for diiron hydroxylase catalysis, including effector protein binding, aromatic substrate binding, electron transfers, O_2 binding, and chemical steps of reaction, is still not completely clear. This timing is complicated in T4MO because of the necessity for two separate protein−protein interactions required to achieve transfers of one electron from T4moC, whereas MMO can potentially accept two electrons from a single protein−protein complex with the FAD and [2Fe-2S]-containing MMO reductase. Single-turnover studies of methane monooxygenase showed *p*-nitrophenol had a k_{off} of ∼0.02 s^{-1}.[72] This rate was comparable to the rate of steady-state turnover of nitrobenzene, suggesting that product release might be rate-determining with this substrate. It has been further suggested that reduction of the MmoH diiron center may promote release of products because of a weakening of the bonding interactions of the phenolate group with the diferrous center and thus prevent release of product more strongly bound to the diferric center from becoming a rate-determining step in catalysis.[72] This hypothesis was supported by a crystallographic study of MmoH bound to 6-bromohexanol, as the product alcohol was not observed in the active site upon reduction of the diiron center in the crystals.[53]

Following this line of reasoning, reduction during the T4MO catalytic cycle may also help to promote release of phenolic products from the diferric resting state, and by overlay of the T4moH−BML and reduced T4moHD structures, Figure 9 suggests a steric contribution to this aspect of the mechanism. During the reduction step, a carboxylate oxygen atom from E231 must move into a bridging position between the iron atoms. By modeling this conversion using the crystal structures of the diferric phenolate-bound product complex (i.e., T4moHD−PCR, PDB entry 3Q14) and the diferrous state (PDB entry 3DHI[37]), we would generate an unfavorable overlap of the migrating carboxylate with the phenolic product. As an alternative to the possible participation in O_2 activation,[37] active site water may also function as a conduit for protonation of the phenolate as it is released from the diiron center. Thus, our structures provide insight into how a redox-driven rearrangement of E231 may assist in displacing the bound product from the diiron center during multiple-turnover catalysis.

dx.doi.org/10.1021/bi2018333 | *Biochemistry* 2012, 51, 1101−1113

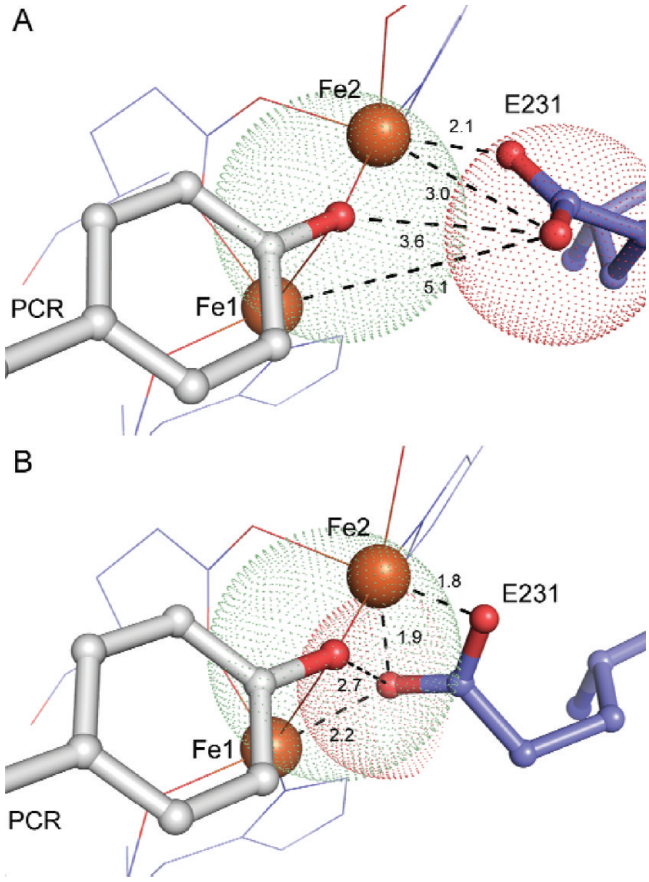

Figure 9. Rearrangement of E231 potentially leading to displacement of an iron-bound product. The images show overlap of the phenolate O of BML and OE2 of E231 upon conversion from the diferric–product complex to the diferrous complex. van der Waals radii of E231 OE2 (red dots) and phenolate O of BML (green dots) are shown. Interatomic distances are shown. (A) Diferric T4moHD–PCR complex (PDB entry 3QI4). (B) Diferrous T4moHD (PDB entry 3DHI).

CONCLUSION

T4moH provides a paradigm for enzymes that perform regiospecific hydroxylation reactions, as the natural active site directs formation of highly reactive intermediates and yields nearly exclusive *para* hydroxylation. The structures presented here lend new insight into the role of complex formation and active site residues in determining this regiospecificity. Additionally, these structures have provided a new view into other aspects of the reactions of T4moH and other diiron hydroxylases, including the role of effector protein in product distributions, the viability of various substrate entrance routes, and a possible structural basis for promoting product release via a redox-gated conformational change of diiron ligand E231.

ASSOCIATED CONTENT

Supporting Information

Residues in the T4moH active site and residues from other diiron hydroxylases in comparable aligned positions (Table S1). This material is available free of charge via the Internet at http://pubs.acs.org.

Accession Codes

Coordinates and structure factors have been deposited in the Protein Data Bank as entries 3RMK (resting T4moH crystals exposed to BML), 3Q14 (resting T4moHD crystallized in the presence of PCR), 3Q3O (resting T4moHD crystallized in the presence of IPH), 3Q3N (resting T4moHD crystallized in the presence of NPO), 3Q3M (resting T4moHD crystallized in the presence of Z82), 3Q2A (resting T4moHD crystallized in the presence of PAB), 3DHH (T4moHD crystals exposed to BML), and 3RI7 (G103L T4moHD).

AUTHOR INFORMATION

Corresponding Author

*Department of Biochemistry, 433 Babcock Dr., University of Wisconsin, Madison, WI 53706. Phone: (608) 262-9708. Fax: (608) 262-3453. E-mail: bgfox@biochem.wisc.edu.

Author Contributions

L.J.B. and J.F.A. contributed equally to this work.

Funding

This work was funded by the National Science Foundation Grants MCB-0316232 and MCB-0843239 to B.G.F.

Notes

The authors declare no competing financial interest.

ACKNOWLEDGMENTS

We thank Dr. Craig A. Bingman (University of Wisconsin Center for Eukaryotic Structural Genomics) for access to crystallography equipment and many useful discussions. The use of the Advanced Photon Source was supported by the U.S. Department of Energy, Basic Energy Sciences, Office of Science, under Contract W-31-109-ENG-38. The use of General Medicine and Cancer Institutes Collaborative Access Team at the Advanced Photon Source was supported by the National Cancer Institute (Y1-CO-1020) and the National Institute of General Medical Sciences (Y1-GM-1104). The use of the Life Science Collaborative Access Team at the Advanced Photon Source was supported by the College of Agricultural and Life Sciences, Department of Biochemistry, and Graduate School of the University of Wisconsin.

ABBREVIATIONS

T4MO, four-protein toluene 4-monooxygenase complex from *Pseudomonas mendocina* KR1; T4moH, hydroxylase component of T4MO; T4moD, effector protein of T4MO; T4moHD, stoichiometric complex of T4moH and T4moD; T4moC, Rieske-type ferredoxin of the T4MO complex; PDB, Protein Data Bank; rmsd, root-mean-square deviation; T4moF, NADH oxidoreductase of the T4MO complex. Abbreviations for aromatic molecules were obtained from the Protein Data Bank Ligand Expo (http://ligand-expo.rcsb.org/): BML, 4-bromophenol; NPO, *p*-nitrophenol; PAB, *p*-NH_2-benzoate; PCR, *p*-cresol; IPH, phenol; Z82, 4-bromobenzoate.

REFERENCES

(1) Green, J., and Dalton, H. (1985) Protein B of soluble methane monooxygenase from *Methylococcus capsulatus* (Bath). A novel regulatory protein of enzyme activity. *J. Biol. Chem. 260*, 15795–15801.

(2) Champreda, V., Choi, Y. J., Zhou, N. Y., and Leak, D. J. (2006) Alteration of the stereo- and regioselectivity of alkene monooxygenase based on coupling protein interactions. *Appl. Microbiol. Biotechnol. 71*, 840–847.

(3) Whited, G. M., and Gibson, D. T. (1991) Separation and partial characterization of the enzymes of the toluene-4-monooxygenase catabolic pathway in *Pseudomonas mendocina* KR1. *J. Bacteriol. 173*, 3017–3020.

(4) Furuya, T., Hirose, S., Osanai, H., Semba, H., and Kino, K. (2010) Identification of the monooxygenase gene clusters that are responsible for the regioselective oxidation of phenol to hydroquinone in *Mycobacteria*. *Appl. Environ. Microbiol. 77*, 1214−1220.
(5) Stubbe, J., and Cotruvo, J. A. Jr. (2011) Control of metallation and active cofactor assembly in the class Ia and Ib ribonucleotide reductases: Diiron or dimanganese? *Curr. Opin. Chem. Biol. 15*, 284−290.
(6) Makris, T. M., Chakrabarti, M., Munck, E., and Lipscomb, J. D. (2010) A family of diiron monooxygenases catalyzing amino acid β-hydroxylation in antibiotic biosynthesis. *Proc. Natl. Acad. Sci. U.S.A. 107*, 15391−15396.
(7) Li, N., Korboukh, V. K., Krebs, C., and Bollinger, J. M. Jr. (2010) Four-electron oxidation of p-hydroxylaminobenzoate to p-nitrobenzoate by a peroxodiferric complex in AurF from *Streptomyces thioluteus*. *Proc. Natl. Acad. Sci. U.S.A. 107*, 15722−15727.
(8) Sobrado, P., Lyle, K. S., Kaul, S., Turco, M. M., Arabshahi, I., Marwah, A., and Fox, B. G. (2006) Identification of the binding region of the [2Fe-2S] ferredoxin in stearoyl-acyl carrier protein desaturase: Insight into the catalytic complex and mechanism of action. *Biochemistry 45*, 4848−4858.
(9) Guy, J. E., Whittle, E., Moche, M., Lengqvist, J., Lindqvist, Y., and Shanklin, J. (2011) Remote control of regioselectivity in acyl-acyl carrier protein-desaturases. *Proc. Natl. Acad. Sci. U.S.A. 108*, 16594−16599.
(10) Krebs, C., Bollinger, J. M. Jr., and Booker, S. J. (2011) Cyanobacterial alkane biosynthesis further expands the catalytic repertoire of the ferritin-like 'di-iron-carboxylate' proteins. *Curr. Opin. Chem. Biol. 15*, 291−303.
(11) Tosha, T., Hasan, M. R., and Theil, E. C. (2008) The ferritin Fe2 site at the diiron catalytic center controls the reaction with O_2 in the rapid mineralization pathway. *Proc. Natl. Acad. Sci. U.S.A. 105*, 18182−18187.
(12) Wiedenheft, B., Mosolf, J., Willits, D., Yeager, M., Dryden, K. A., Young, M., and Douglas, T. (2005) An archaeal antioxidant: Characterization of a Dps-like protein from *Sulfolobus solfataricus*. *Proc. Natl. Acad. Sci. U.S.A. 102*, 10551−10556.
(13) Cooley, R. B., Arp, D. J., and Karplus, P. A. (2011) Symerythrin structures at atomic resolution and the origins of rubrerythrins and the ferritin-like superfamily. *J. Mol. Biol. 413*, 177−194.
(14) Stenmark, P., Grunler, J., Mattsson, J., Sindelar, P. J., Nordlund, P., and Berthold, D. A. (2001) A new member of the family of di-iron carboxylate proteins. Coq7 (clk-1), a membrane-bound hydroxylase involved in ubiquinone biosynthesis. *J. Biol. Chem. 276*, 33297−33300.
(15) Mathevon, C., Pierrel, F., Oddou, J. L., Garcia-Serres, R., Blondin, G., Latour, J. M., Menage, S., Gambarelli, S., Fontecave, M., and Atta, M. (2007) tRNA-modifying MiaE protein from *Salmonella typhimurium* is a nonheme diiron monooxygenase. *Proc. Natl. Acad. Sci. U.S.A. 104*, 13295−13300.
(16) Bollinger, J. M. Jr., Diao, Y., Matthews, M. L., Xing, G., and Krebs, C. (2009) myo-Inositol oxygenase: A radical new pathway for O_2 and C-H activation at a nonheme diiron cluster. *Dalton Trans.*, 905−914.
(17) Vu, V. V., Emerson, J. P., Martinho, M., Kim, Y. S., Munck, E., Park, M. H., and Que, L. Jr. (2009) Human deoxyhypusine hydroxylase, an enzyme involved in regulating cell growth, activates O_2 with a nonheme diiron center. *Proc. Natl. Acad. Sci. U.S.A. 106*, 14814−14819.
(18) Behan, R. K., and Lippard, S. J. (2010) The aging-associated enzyme CLK-1 is a member of the carboxylate-bridged diiron family of proteins. *Biochemistry 49*, 9679−9681.
(19) Yamashita, M., Furutachi, H., Tosha, T., Fujinami, S., Saito, W., Maeda, Y., Takahashi, K., Tanaka, K., Kitagawa, T., and Suzuki, M. (2007) Regioselective arene hydroxylation mediated by a (μ-peroxo)diiron(III) complex: A functional model for toluene monooxygenase. *J. Am. Chem. Soc. 129*, 2−3.
(20) Bell, C. B., Calhoun, J. R., Bobyr, E., Wei, P. P., Hedman, B., Hodgson, K. O., Degrado, W. F., and Solomon, E. I. (2009) Spectroscopic definition of the biferrous and biferric sites in de novo designed four-helix bundle DFsc peptides: Implications for O_2 reactivity of binuclear non-heme iron enzymes. *Biochemistry 48*, 59−73.
(21) Xue, G., De Hont, R., Munck, E., and Que, L. Jr. (2010) Million-fold activation of the [$Fe_2(\mu$-$O)_2$] diamond core for C-H bond cleavage. *Nat. Chem. 2*, 400−405.
(22) Friedle, S., Reisner, E., and Lippard, S. J. (2010) Current challenges of modeling diiron enzyme active sites for dioxygen activation by biomimetic synthetic complexes. *Chem. Soc. Rev. 39*, 2768−2779.
(23) Do, L. H., Hayashi, T., Moenne-Loccoz, P., and Lippard, S. J. (2010) Carboxylate as the protonation site in (peroxo)diiron(III) model complexes of soluble methane monooxygenase and related diiron proteins. *J. Am. Chem. Soc. 132*, 1273−1275.
(24) Xue, G., Pokutsa, A., and Que, L. Jr. (2011) Substrate-triggered activation of a synthetic [$Fe_2(\mu$-$O)_2$] diamond core for C-H bond cleavage. *J. Am. Chem. Soc. 133*, 16657−16667.
(25) Yen, K. M., Karl, M. R., Blatt, L. M., Simon, M. J., Winter, R. B., Fausset, P. R., Lu, H. S., Harcourt, A. A., and Chen, K. K. (1991) Cloning and characterization of a *Pseudomonas mendocina* KR1 gene cluster encoding toluene-4-monooxygenase. *J. Bacteriol. 173*, 5315−5327.
(26) Oppenheim, S. F., Studts, J. M., Fox, B. G., and Dordick, J. S. (2001) Aromatic hydroxylation catalyzed by toluene 4-monooxygenase in organic solvent/aqueous buffer mixtures. *Appl. Biochem. Biotechnol. 90*, 187−197.
(27) Tao, Y., Fishman, A., Bentley, W. E., and Wood, T. K. (2004) Altering toluene 4-monooxygenase by active-site engineering for the synthesis of 3-methoxycatechol, methoxyhydroquinone, and methylhydroquinone. *J. Bacteriol. 186*, 4705−4713.
(28) McClay, K., Boss, C., Keresztes, I., and Steffan, R. J. (2005) Mutations of toluene-4-monooxygenase that alter regiospecificity of indole oxidation and lead to production of novel indigoid pigments. *Appl. Environ. Microbiol. 71*, 5476−5483.
(29) Feingersch, R., Shainsky, J., Wood, T. K., and Fishman, A. (2008) Protein engineering of toluene monooxygenases for synthesis of chiral sulfoxides. *Appl. Environ. Microbiol. 74*, 1555−1566.
(30) Notomista, E., Scognamiglio, R., Troncone, L., Donadio, G., Pezzella, A., Di Donato, A., and Izzo, V. (2011) Tuning the specificity of the recombinant multicomponent toluene o-xylene monooxygenase from *Pseudomonas* sp. strain OX1 for the biosynthesis of tyrosol from 2-phenylethanol. *Appl. Environ. Microbiol. 77*, 5428−5437.
(31) Tinberg, C. E., and Lippard, S. J. (2011) Dioxygen activation in soluble methane monooxygenase. *Acc. Chem. Res. 44*, 280−288.
(32) Fox, B. G. (1998) Catalysis by non-heme iron-containing enzymes. In *Comprehensive Biological Catalysis* (Sinnott, M., Ed.) pp 261−348, Academic Press, London.
(33) Rosenzweig, A. C., Frederick, C. A., Lippard, S. J., and Nordlund, P. (1993) Crystal structure of a bacterial non-haem iron hydroxylase that catalyses the biological oxidation of methane. *Nature 366*, 537−543.
(34) Elango, N., Radhakrishnan, R., Froland, W. A., Wallar, B. J., Earhart, C. A., Lipscomb, J. D., and Ohlendorf, D. H. (1997) Crystal structure of the hydroxylase component of methane monooxygenase from *Methylosinus trichosporium* OB3b. *Protein Sci. 6*, 556−568.
(35) Sazinsky, M. H., Bard, J., Di Donato, A., and Lippard, S. J. (2004) Crystal structure of the toluene/o-xylene monooxygenase hydroxylase from *Pseudomonas stutzeri* OX1. Insight into the substrate specificity, substrate channeling, and active site tuning of multicomponent monooxygenases. *J. Biol. Chem. 279*, 30600−30610.
(36) Sazinsky, M. H., Dunten, P. W., McCormick, M. S., DiDonato, A., and Lippard, S. J. (2006) X-ray structure of a hydroxylase-regulatory protein complex from a hydrocarbon-oxidizing multicomponent monooxygenase, *Pseudomonas* sp. OX1 phenol hydroxylase. *Biochemistry 45*, 15392−15404.
(37) Bailey, L. J., McCoy, J. G., Phillips, G. N. Jr., and Fox, B. G. (2008) Structural consequences of effector protein complex formation in a diiron hydroxylase. *Proc. Natl. Acad. Sci. U.S.A. 105*, 19194−19198.

(38) Lipscomb, J. D. (1994) Biochemistry of the soluble methane monooxygenase. *Annu. Rev. Microbiol. 48*, 371−399.
(39) Fox, B. G., Liu, Y., Dege, J. E., and Lipscomb, J. D. (1991) Complex formation between the protein components of methane monooxygenase from *Methylosinus trichosporium* OB3b. Identification of sites of component interaction. *J. Biol. Chem. 266*, 540−550.
(40) Mitchell, K. H., Studts, J. M., and Fox, B. G. (2002) Combined participation of hydroxylase active site residues and effector protein binding in a para to ortho modulation of toluene 4-monooxygenase regiospecificity. *Biochemistry 41*, 3176−3188.
(41) Lountos, G. T., Mitchell, K. H., Studts, J. M., Fox, B. G., and Orville, A. M. (2005) Crystal structures and functional studies of T4moD, the toluene 4-monooxygenase catalytic effector protein. *Biochemistry 44*, 7131−7142.
(42) Pikus, J. D., Studts, J. M., Achim, C., Kauffmann, K. E., Munck, E., Steffan, R. J., McClay, K., and Fox, B. G. (1996) Recombinant toluene-4-monooxygenase: Catalytic and Mossbauer studies of the purified diiron and Rieske components of a four-protein complex. *Biochemistry 35*, 9106−9119.
(43) Pikus, J. D., Studts, J. M., McClay, K., Steffan, R. J., and Fox, B. G. (1997) Changes in the regiospecificity of aromatic hydroxylation produced by active site engineering in the diiron enzyme toluene 4-monooxygenase. *Biochemistry 36*, 9283−9289.
(44) Pikus, J. D., Mitchell, K. H., Studts, J. M., McClay, K., Steffan, R. J., and Fox, B. G. (2000) Threonine 201 in the diiron enzyme toluene 4-monooxygenase is not required for catalysis. *Biochemistry 39*, 791−799.
(45) Moe, L. A., Hu, Z., Deng, D., Austin, R. N., Groves, J. T., and Fox, B. G. (2004) Remarkable aliphatic hydroxylation by the diiron enzyme toluene 4-monooxygenase in reactions with radical or cation diagnostic probes norcarane, 1,1-dimethylcyclopropane, and 1,1-diethylcyclopropane. *Biochemistry 43*, 15688−15701.
(46) Rui, L., Kwon, Y. M., Fishman, A., Reardon, K. F., and Wood, T. K. (2004) Saturation mutagenesis of toluene ortho-monooxygenase of *Burkholderia cepacia* G4 for enhanced 1-naphthol synthesis and chloroform degradation. *Appl. Environ. Microbiol. 70*, 3246−3252.
(47) Vardar, G., and Wood, T. K. (2004) Protein engineering of toluene-o-xylene monooxygenase from *Pseudomonas stutzeri* OX1 for synthesizing 4-methylresorcinol, methylhydroquinone, and pyrogallol. *Appl. Environ. Microbiol. 70*, 3253−3262.
(48) Elsen, N. L., Bailey, L. J., Hauser, A. D., and Fox, B. G. (2009) Role for threonine 201 in the catalytic cycle of the soluble diiron hydroxylase toluene 4-monooxygenase. *Biochemistry 48*, 3838−3846.
(49) Fishman, A., Tao, Y., Bentley, W. E., and Wood, T. K. (2004) Protein engineering of toluene 4-monooxygenase of *Pseudomonas mendocina* KR1 for synthesizing 4-nitrocatechol from nitrobenzene. *Biotechnol. Bioeng. 87*, 779−790.
(50) Vardar, G., Tao, Y., Lee, J., and Wood, T. K. (2005) Alanine 101 and alanine 110 of the α subunit of *Pseudomonas stutzeri* OX1 toluene-o-xylene monooxygenase influence the regiospecific oxidation of aromatics. *Biotechnol. Bioeng. 92*, 652−658.
(51) Tao, Y., Bentley, W. E., and Wood, T. K. (2005) Regiospecific oxidation of naphthalene and fluorene by toluene monooxygenases and engineered toluene 4-monooxygenases of *Pseudomonas mendocina* KR1. *Biotechnol. Bioeng. 90*, 85−94.
(52) Froland, W. A., Andersson, K. K., Lee, S. K., Liu, Y., and Lipscomb, J. D. (1992) Methane monooxygenase component B and reductase alter the regioselectivity of the hydroxylase component-catalyzed reactions. A novel role for protein-protein interactions in an oxygenase mechanism. *J. Biol. Chem. 267*, 17588−17597.
(53) Sazinsky, M. H., and Lippard, S. J. (2005) Product bound structures of the soluble methane monooxygenase hydroxylase from *Methylococcus capsulatus* (Bath): Protein motion in the α-subunit. *J. Am. Chem. Soc. 127*, 5814−5825.
(54) Studts, J. M., Mitchell, K. H., Pikus, J. D., McClay, K., Steffan, R. J., and Fox, B. G. (2000) Optimized expression and purification of toluene 4-monooxygenase hydroxylase. *Protein Expression Purif. 20*, 58−65.
(55) Moe, L. A., Bingman, C. A., Wesenberg, G. E., Phillips, G. N. Jr., and Fox, B. G. (2006) Structure of T4moC, the Rieske-type ferredoxin component of toluene 4-monooxygenase. *Acta Crystallogr. D62*, 476−482.
(56) Bailey, L. J., Elsen, N. L., Pierce, B. S., and Fox, B. G. (2007) Soluble expression and purification of the oxidoreductase component of toluene 4-monooxygenase. *Protein Expression Purif. 57*, 9−16.
(57) Otwinowski, Z., and Minor, W. (1997) The processing of X-ray diffraction data collected in oscillation mode. *Methods Enzymol. 276*, 307−326.
(58) Vagin, A., and Teplyakov, A. (1997) MOLREP: An automated program for molecular replacement. *J. Appl. Crystallogr. 30*, 1022−1025.
(59) Emsley, P., and Cowtan, K. (2004) Coot: Model-building tools for molecular graphics. *Acta Crystallogr. D60*, 2126−2132.
(60) Vagin, A. A., Steiner, R. A., Lebedev, A. A., Potterton, L., McNicholas, S., Long, F., and Murshudov, G. N. (2004) REFMAC5 dictionary: Organization of prior chemical knowledge and guidelines for its use. *Acta Crystallogr. D60*, 2184−2195.
(61) Murshudov, G. N., Vagin, A. A., and Dodson, E. J. (1997) Refinement of macromolecular structures by the maximum-likelihood method. *Acta Crystallogr. D53*, 240−255.
(62) Lovell, S. C., Davis, I. W., Arendall, W. B. III, de Bakker, P. I., Word, J. M., Prisant, M. G., Richardson, J. S., and Richardson, D. C. (2003) Structure validation by Cα geometry: ϕ, ψ and Cβ deviation. *Proteins 50*, 437−450.
(63) Petrek, M., Otyepka, M., Banas, P., Kosinova, P., Koca, J., and Damborsky, J. (2006) CAVER: A new tool to explore routes from protein clefts, pockets and cavities. *BMC Bioinf. 7*, 316.
(64) DeLano, W. L. (2002) *The PyMOL Molecular Graphics System*, DeLano Scientific, San Carlos, CA.
(65) Andersson, K. K., Elgren, T. E., Que, L. J., and Lipscomb, J. D. (1992) Accessibility to the active site of methane monooxygenase: The first demonstration of exogenous ligand binding to the diiron cluster. *J. Am. Chem. Soc. 114*, 8711−8713.
(66) Whittington, D. A., Rosenzweig, A. C., Frederick, C. A., and Lippard, S. J. (2001) Xenon and halogenated alkanes track putative substrate binding cavities in the soluble methane monooxygenase hydroxylase. *Biochemistry 40*, 3476−3482.
(67) Schwartz, J. K., Wei, P. P., Mitchell, K. H., Fox, B. G., and Solomon, E. I. (2008) Geometric and electronic structure studies of the binuclear nonheme ferrous active site of toluene-4-monooxygenase: Parallels with methane monooxygenase and insight into the role of the effector proteins in O_2 activation. *J. Am. Chem. Soc. 130*, 7098−7109.
(68) Murray, L. J., Garcia-Serres, R., McCormick, M. S., Davydov, R., Naik, S. G., Kim, S. H., Hoffman, B. M., Huynh, B. H., and Lippard, S. J. (2007) Dioxygen activation at non-heme diiron centers: Oxidation of a proximal residue in the I100W variant of toluene/o-xylene monooxygenase hydroxylase. *Biochemistry 46*, 14795−14809.
(69) Lovell, S. C., Word, J. M., Richardson, J. S., and Richardson, D. C. (2000) The penultimate rotamer library. *Proteins 40*, 389−408.
(70) Song, W. J., Gucinski, G., Sazinsky, M. H., and Lippard, S. J. (2011) Tracking a defined route for O_2 migration in a dioxygen-activating diiron enzyme. *Proc. Natl. Acad. Sci. U.S.A. 108*, 14795−14800.
(71) McCormick, M. S., and Lippard, S. J. (2011) Analysis of substrate access to active sites in bacterial multicomponent monooxygenase hydroxylases: X-ray crystal structure of xenon-pressurized phenol hydroxylase from *Pseudomonas* sp. OX1. *Biochemistry 50*, 11058−11069.
(72) Lee, S. K., Nesheim, J. C., and Lipscomb, J. D. (1993) Transient intermediates of the methane monooxygenase catalytic cycle. *J. Biol. Chem. 268*, 21569−21577.
(73) Beauvais, L. G., and Lippard, S. J. (2005) Reactions of the peroxo intermediate of soluble methane monooxygenase hydroxylase with ethers. *J. Am. Chem. Soc. 127*, 7370−7378.
(74) Murray, L. J., Naik, S. G., Ortillo, D. O., Garcia-Serres, R., Lee, J. K., Huynh, B. H., and Lippard, S. J. (2007) Characterization of the

arene-oxidizing intermediate in ToMOH as a diiron(III) species. *J. Am. Chem. Soc. 129*, 14500−14510.
(75) Mitchell, K. H., Rogge, C. E., Gierahn, T., and Fox, B. G. (2003) Insight into the mechanism of aromatic hydroxylation by toluene 4-monooxygenase by use of specifically deuterated toluene and *p*-xylene. *Proc. Natl. Acad. Sci. U.S.A. 100*, 3784−3789.
(76) Brazeau, B. J., and Lipscomb, J. D. (2003) Key amino acid residues in the regulation of soluble methane monooxygenase catalysis by component B. *Biochemistry 42*, 5618−5631.
(77) Newman, L. M., and Wackett, L. P. (1995) Purification and characterization of toluene 2-monooxygenase from *Burkholderia cepacia* G4. *Biochemistry 34*, 14066−14076.
(78) Cafaro, V., Scognamiglio, R., Viggiani, A., Izzo, V., Passaro, I., Notomista, E., Piaz, F. D., Amoresano, A., Casbarra, A., Pucci, P., and Di Donato, A. (2002) Expression and purification of the recombinant subunits of toluene/o-xylene monooxygenase and reconstitution of the active complex. *Eur. J. Biochem. 269*, 5689−5699.
(79) Moe, L. A. (2005) Catalytic Studies and Component Interactions of the Toluene 4-Monooxygenase from *Pseudomonas mendocina* KR1. Ph.D. Thesis, University of Wisconsin, Madison, WI.
(80) Bailey, L. J., and Fox, B. G. (2009) Crystallographic and catalytic studies of the peroxide-shunt reaction in a diiron hydroxylase. *Biochemistry 48*, 8932−8939.
(81) Shu, L., Nesheim, J. C., Kauffmann, K., Munck, E., Lipscomb, J. D., and Que, L. Jr. (1997) An $Fe_2^{IV}O_2$ diamond core structure for the key intermediate Q of methane monooxygenase. *Science 275*, 515−518.